Park, J., Lühr, H., Nishioka, M., Kwak, Y.-S. (2015): Plasma density undulations correlated with thermospheric neutral mass density in the daytime low-latitude to midlatitude topside ionosphere. - *Journal of Geophysical Research*, *120*, 8, pp. 6669—6678.

DOI: http://doi.org/10.1002/2015JA021525

AGU PUBLICATIONS

JGR

Journal of Geophysical Research: Space Physics

RESEARCH ARTICLE
10.1002/2015JA021525

Key Points:
- There are plasma density undulations that correlated well with neutral mass density
- The relative amplitudes are larger in the winter hemisphere
- The relative amplitudes depend weakly on solar activity

Correspondence to:
J. Park,
pj@kasi.re.kr

Citation:
Park, J., H. Lühr, M. Nishioka, and Y.-S. Kwak (2015), Plasma density undulations correlated with thermospheric neutral mass density in the daytime low-latitude to midlatitude topside ionosphere, *J. Geophys. Res. Space Physics*, *120*, 6669–6678, doi:10.1002/2015JA021525.

Received 1 JUN 2015
Accepted 4 JUL 2015
Accepted article online 7 JUL 2015
Published online 4 AUG 2015

Plasma density undulations correlated with thermospheric neutral mass density in the daytime low-latitude to midlatitude topside ionosphere

Jaeheung Park[1], Hermann Lühr[2], Michi Nishioka[3], and Young-Sil Kwak[1,4]

[1]Korea Astronomy and Space Science Institute, Daejeon, South Korea, [2]Helmholtz Centre Potsdam GFZ German Research Centre for Geosciences, Potsdam, Germany, [3]National Institute of Information and Communications Technology, Tokyo, Japan, [4]Department of Astronomy and Space Science, University of Science and Technology, Daejeon, South Korea

Abstract Plasma density undulations in the dayside low-latitude/midlatitude ionospheric *F* region were often attributed to thermospheric gravity waves (TGWs). However, the relationship between the former and the latter has been at best indirectly evidenced. In this study we investigate daytime fluctuations in neutral mass density (ρ) and plasma density (n_e) measured onboard CHAMP from 2001 to 2010. A significant amount of daytime fluctuations in n_e is strongly correlated with in situ fluctuations of ρ, which we term "TGW-related n_e fluctuations." The TGW-related n_e fluctuations are (1) stronger in the winter hemisphere than in the summer hemisphere and (2) strongest in the South American sector during June solstice months. These climatological features are in general agreement with those of TGWs reported previously, especially at midlatitudes. On the other hand, the relative amplitude of TGW-related n_e fluctuations does not depend strongly on solar activity.

1. Introduction

Many observational studies addressed plasma density undulation in the dayside ionospheric *F* region [e.g., *Kotake et al.*, 2006; *Ishida et al.*, 2008; *Morgan*, 1990; *Retterer and Roddy*, 2014]. The daytime plasma density undulations in the ionosphere were often attributed to thermospheric gravity waves (TGWs) [e.g., *Kotake et al.*, 2007; *Otsuka et al.*, 2013; *Nishioka et al.*, 2013; *Vadas and Liu*, 2013]. However, the relation between the former (plasma undulations) and the latter (TGWs) has been at best indirectly inferred: from simulations and/or circumstantial evidences. Admittedly, the indirect/circumstantial evidences are quite persuasive for some of the studies. For example, downward phase propagation of daytime ionospheric disturbances, such as given in *Hocke et al.* [1996], *Nicolls and Heinselman* [2007], and *Nygrén et al.* [2015], may be a plausible evidence that they originate from TGWs. *Nishioka et al.* [2013] observed (a) concentric ring signatures in total electron content (TEC) and (b) the existence of a tornado near the ring center. From backward ray tracing those authors confirmed the relationship between (a) and (b), which strongly supported the inference that the tornado-related TGWs led to the TEC perturbations. Nevertheless, no study has ever confirmed that the observed fluctuations in ionospheric plasma density are actually accompanied by similar fluctuations in thermospheric (neutral) mass density at the same location.

Likewise, some previous papers addressed fluctuations of thermospheric quantities at *F* region altitudes using in situ neutral component observations but showed no decisive evidence of accompanying fluctuations in *F* region plasma density [e.g., *Johnson et al.*, 1995; *Forbes et al.*, 2008; *Liu et al.*, 2009; *Fedorenko*, 2010; *Fedorenko and Kryuchkov*, 2014; *Park et al.*, 2014; *Fedorenko et al.*, 2015]. A comparison between *F* region ionospheric fluctuations and *E* region atmospheric gravity waves (AGWs) at high latitudes has been conducted by *Nygrén et al.* [2015]. However, the comparison was not conducted at the same altitude, and their neutral wind data do not originate from direct observations of neutral particles but indirectly from beam-aligned ion velocity profiles derived from the European Incoherent Scatter Scientific Association (EISCAT) data. Comparative studies on neutral and plasma fluctuations have been conducted in the Venusian thermosphere [e.g., *Hoegy et al.*, 1990] and in the terrestrial mesosphere [e.g., *Lübken et al.*, 1993]. As far as the authors know, however, there has been no comparative study in the terrestrial dayside low-latitude/midlatitude ionosphere and thermosphere at *F* region altitudes.

In this study we are going to address the two scientific questions. First, is there any plasma density fluctuation in the daytime low-latitude/midlatitude ionosphere actually accompanied by TGWs (or simply neutral density perturbations in a broad sense)? Second, if such ionospheric perturbations do exist, what is their global and seasonal distribution? These questions will be answered using in situ observations of plasma density and neutral mass density on board the Challenging Mini-Satellite Payload (CHAMP).

2. Instruments and Analysis Methods

The CHAMP satellite was launched in July 2000 into a circular (initial altitude ~450 km) and polar (inclination angle ~87.3°) orbit. It carried a Planar Langmuir Probe (PLP) to measure electron density (≈ plasma density) and temperature and an accelerometer (ACC) from which to estimate neutral mass density. The nominal data rate is once per 15 s (once per 10 s) for the PLP (ACC). To synchronize the two data sets, we resample the PLP and ACC data at 5 s cadence using linear interpolation.

Figures 1a and 1b present an example of neutral mass density (ρ, normalized to the 400 km altitude) and plasma density (n_e), respectively, resampled from CHAMP observations every 5 s. In order to isolate fluctuating components from these two time series, we first subtract background variations ($\rho^{\text{background}}$ and $n_e^{\text{background}}$) from the original time series. We obtain the background variation by low-pass filtering with a Savitzky-Golay filter of order 3 and a window size of 115 s. The cutoff period of the background removal procedure is defined as the period of a sinusoidal wave for which the ratio between input and output root-mean-square (RMS) levels is 0.707. This cutoff period can be converted into a cutoff scale if we consider the orbital speed of 7.5 km/s. The cutoff wavelength is estimated to be approximately 600 km along the CHAMP track. Note that this cutoff scale is similar to that used in *Park et al.* [2014]. According to the Nyquist theorem, the smallest resolvable scale length in this study is twice the resampling cadence (5 s) times the orbital speed (7.5 km/s), which is 75 km. Therefore, this study investigates fluctuations within the scale length range from 75 km to 600 km.

Second, the residuals (i.e., $\delta\rho = \rho - \rho^{\text{background}}$ and $\delta n_e = n_e - n_e^{\text{background}}$) are normalized by the respective background values (i.e., $\rho^{\text{background}}$ and $n_e^{\text{background}}$) to obtain the relative fluctuation levels given in Figure 1c. Then we cross-correlate the normalized fluctuations of ρ and n_e within a 355 s (= ±35 data points for the 5 s cadence) window advancing the center points in steps of 5 s. The CHAMP data sets are divided into daily files, and zero correlation coefficients are assigned to the first and last 35 data points of a day. As there can be phase differences between fluctuations in plasma and neutral densities [*Onishi et al.*, 2009, Figure 3], we allow arbitrary phase offsets between the two quantities and take the maximum cross-correlation coefficient within each window as the representative value (Figure 1d). Note that variable phase offsets between plasma and neutral density fluctuations can also be found in the Venusian ionosphere/thermosphere [*Hoegy et al.*, 1990]. If the maximum correlation coefficient is higher than 0.7 (the horizontal dashed line in Figure 1d), the corresponding $\delta n_e/n_e^{\text{background}}$ is deemed to originate from $\delta\rho/\rho^{\text{background}}$, which we term "TGW-related n_e fluctuations." Plasma density fluctuations which are poorly correlated with neutral mass density fluctuations (as seen poleward of 10°N in Figure 1d) are neglected in the following processes. For example, the plasma density fluctuation is strong in the region poleward of 60°N in Figure 1 while its correlation with the neutral mass density fluctuation is low.

By this cross-correlation method we reduce the risk of interpreting instrument noise in n_e divided by a small $n_e^{\text{background}}$ as valid n_e fluctuation. Note also that the maximum cross-correlation coefficients given in Figure 1d do not depend on the amplitude of neutral mass density fluctuations. In other words, TGW-related n_e fluctuations (Figure 1e) do not necessarily coincide with strong fluctuations in neutral mass density (Figure 1c).

We then calculate bin averages of the TGW-related n_e fluctuations (represented by $|\delta n_e/n_e^{\text{background}}|$ as shown in Figure 1e) where each bin spans 5° in geographic latitude (GLAT) by 5° in geographic longitude (GLON) for each season. June and December seasons are defined as 131 days centered around June and December solstice, respectively. Combined equinoxes are defined as a combination of 65 days around each equinox day. A period of about 130 days is needed for CHAMP to cover all local time (LT) sectors.

Equatorial plasma bubbles (EPBs) and nighttime medium-scale traveling ionospheric disturbances (MSTIDs) are known to cause fluctuations of plasma density in the nighttime ionosphere. It is generally accepted that these phenomena are generated by plasma instability mechanisms (albeit with initial seeding from AGWs) [e.g., *Yokoyama and Hysell*, 2010; *Yokoyama et al.*, 2014; *Kil*, 2015] rather than driven directly by AGWs. In order

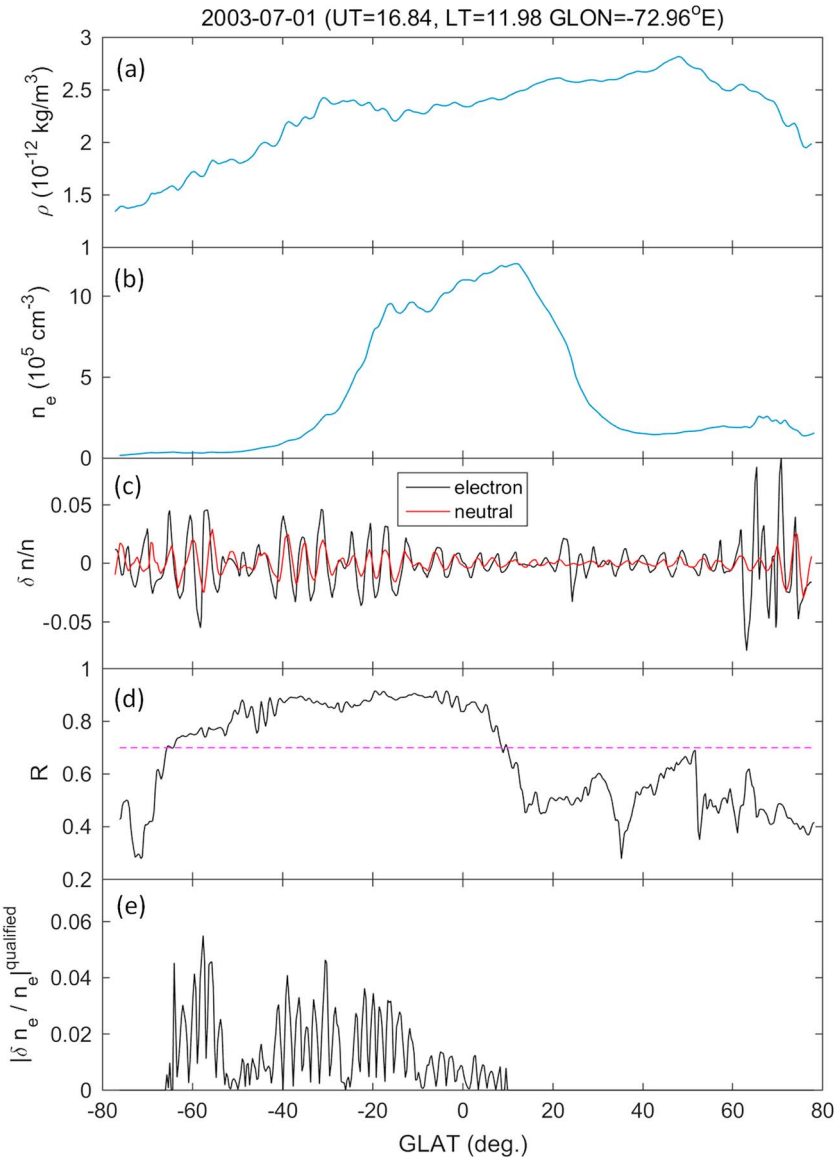

Figure 1. An example data recorded by CHAMP: (a) neutral mass density, (b) plasma density, (c) relative fluctuation amplitudes of mass density and plasma density, (d) maximum cross-correlation coefficient between mass density and plasma density fluctuation, and (e) relative fluctuation amplitude of plasma density when the maximum cross-correlation coefficient exceeds 0.7.

to avoid plasma density fluctuations related to EPBs or nighttime MSTIDs, we concentrate on daytime hours from 09 to 18 h in LT.

3. Statistical Results

For the analysis of CHAMP data we used years 2001–2010 in order to find out the average features of plasma density fluctuations during solar maximum and minimum conditions. In this study we focus on the low-latitude/midlatitude ionosphere ($|\mathrm{MLAT}| \leq 60°$) on the dayside. Higher-latitude regions are not considered in the following because of their proximity to the polar cusp. Both ionospheric plasma density [e.g., *Goodwin et al.*, 2015] and thermospheric mass density [e.g., *Lühr et al.*, 2004] are frequently modulated in the cusp, generally by processes occurring near the dayside magnetopause. However, the thermospheric/ionospheric disturbances by the cusp are beyond the scope of this study.

Figure 2 shows bin-averaged amplitudes of TGW-related n_e fluctuations (as shown in Figure 1e) during the solar minimum years (2006–2010), which are smoothed by a 5×5 two-dimensional median filter. Each panel

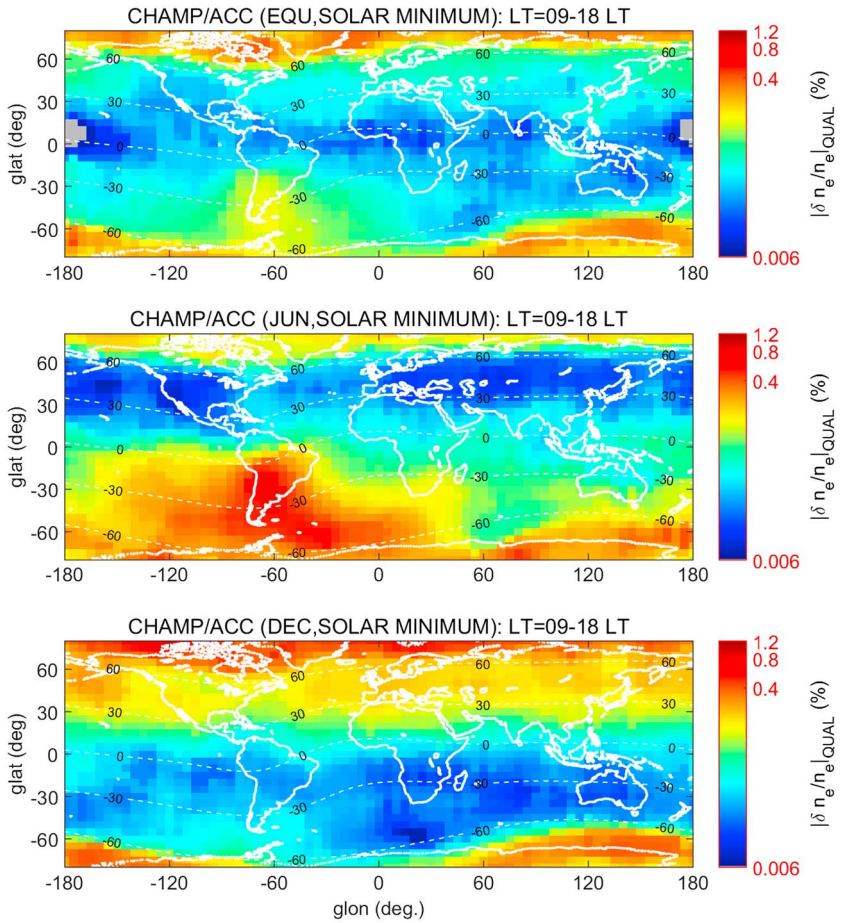

Figure 2. Bin-averaged amplitudes of TGW-related n_e fluctuations during solar minimum years (2006–2010). (from top to bottom) Equinox, June solstice, and December solstice results.

from top to bottom corresponds to combined equinoxes, June solstice, and December solstice, respectively. During solstices (Figures 2, middle, and 2, bottom) the winter hemisphere exhibits stronger fluctuations in plasma density than the summer hemisphere. Plasma density fluctuations are stronger in South America during June solstice than at any other location and season.

Figure 3 is the same as Figure 2 but for solar maximum years from 2001 to 2005. Overall, the level of plasma density fluctuations in Figure 3 is comparable to that of Figure 2. The two key features in Figure 2 (preference for the winter hemisphere and the hottest spot above South America in June) can also be identified in Figure 3. When we calculate averages of relative plasma density fluctuations over the latitude range of ±60° MLAT, the ratio between solar minimum (Figure 2) and maximum (Figure 3) is below 1.3.

4. Discussion

In the previous section we have shown that the TGW-related n_e variations show distinct spatial distributions which change with season. Here we will try to interpret these observations and compare them with previous studies.

4.1. Plasma Density Fluctuations Resulting From In Situ Neutral Density Undulations

Besides the plasma density undulations correlated with neutral perturbations (as shown in Figures 2 and 3) there exist other populations of plasma variations. For example, some AGWs may dissipate between the *E* and *F* regions. Mass density variations of those AGWs are invisible at *F* region altitudes, but they affect the *E* region dynamo, and in response the resultant *E* field can perturb the *F* region plasma density. There are also other origins for apparent fluctuations in the in situ plasma density profile. It is known that a step function is equivalent to a superposition of sinusoidal waves over a wide range of wavelength. When the step function

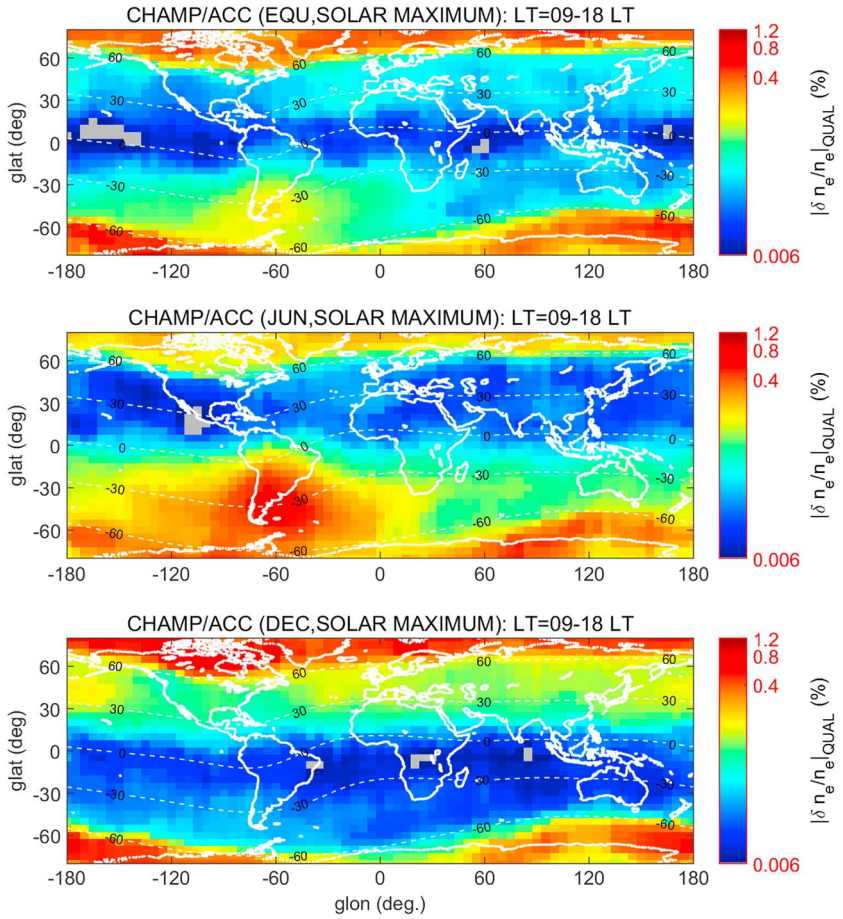

Figure 3. The same as Figure 2, but for solar maximum years (2001–2005).

is high-pass filtered, the output signal shows fluctuations with appreciable amplitudes. Therefore, steep density gradients, e.g., those related with the equatorial ionization anomaly (EIA), lead to fluctuations when they are filtered by the procedure described in section 2 (see ~22°N in Figure 1). Instrument noise can also cause artificial fluctuations in $\delta n_e/n_e^{\text{background}}$ when the background density ($n_e^{\text{background}}$) is very low. Our analysis approach helps to suppress most of the signals mentioned above.

The results in section 3 show that a good part of the daytime fluctuations in ionospheric plasma density is correlated with in situ fluctuations of neutral mass density. A high correlation between plasma and neutral density fluctuations may not necessarily imply a cause and effect relationship. However, if we consider previous theoretical works which supported ionospheric disturbance by TGWs [e.g., *Vadas and Liu*, 2013], the good correlation is in favor of a cause and effect relationship between the two quantities. Note that the horizontal wave lengths investigated in *Vadas and Liu* [2013] were of the order of 1000 km, which is much larger than the ones analyzed in our study. As for the horizontal wave length range of our interest here (75–600 km), *Vadas* [2007, Figure 9b] shows that uppermost dissipation altitudes of TGWs are approximately 200–400 km. Since the dissipation altitude is the height of maximum momentum flux, TGWs whose wave lengths are between 75 km and 600 km can penetrate to altitudes even higher than 200–400 km, possibly up to and beyond CHAMP altitudes. Those TGWs are also expected to generate ionospheric disturbances via field-aligned ion transport by neutral particles, as inferred for large-scale (horizontal wave length of the order of 1000 km) TGWs by *Vadas and Liu* [2013]. Hence, we can deduce from *Vadas* [2007] and *Vadas and Liu* [2013] that TGWs are a plausible cause for the plasma density undulations observed by CHAMP.

4.2. Comparison With Data From Ground-Based Instruments

For further interpretation of our results, we have searched for coincident observations between CHAMP and ground-based receivers of Global Navigation Satellite System (GNSS) signals. The GNSS Earth Observation Network System (GEONET) consists of receiver arrays in Japan, and we can get TEC maps around the islands

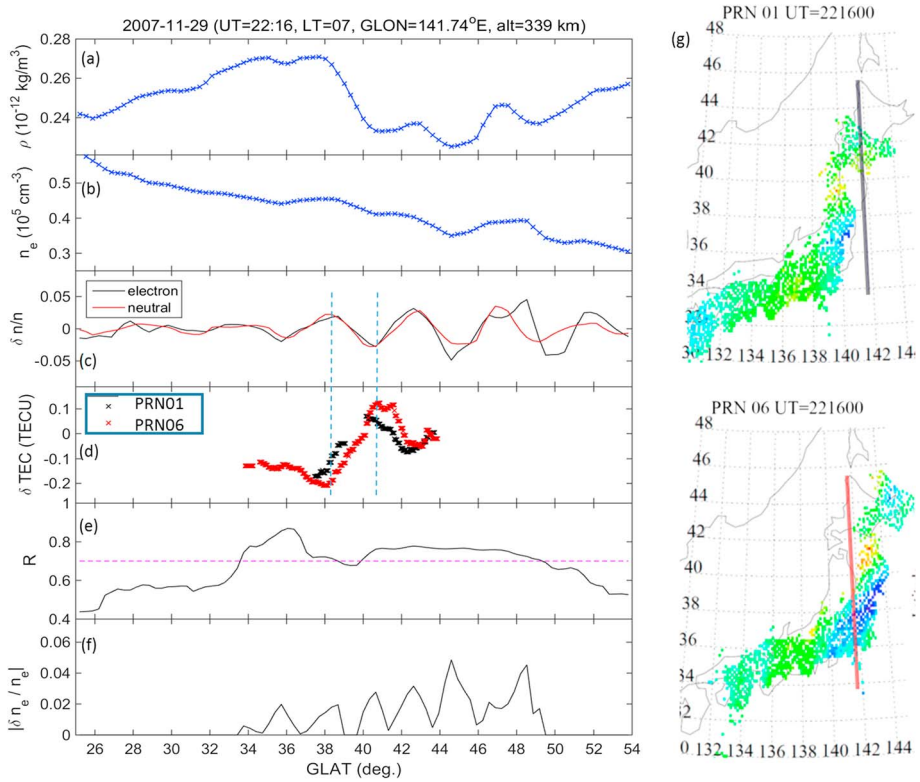

Figure 4. Collocated observations of CHAMP and GEONET from 29 November 2007. (a) Neutral mass density, (b) plasma density, (c) relative fluctuation amplitudes of neutral mass density and plasma density, (d) GEONET TEC fluctuations resampled along the CHAMP track, (e) maximum cross-correlation coefficient between relative fluctuation amplitudes of neutral mass density and plasma density, and (f) relative fluctuation amplitude of plasma density when the maximum cross-correlation coefficient exceeds 0.7. (g) GEONET 2-D TEC maps obtained from the GNSS Pseudo Random Number (PRN) 01 and PRN 06. The CHAMP track is marked as thick solid lines in Figure 4g.

with high spatial and temporal resolution. Figure 4 shows an example of coincident observations of CHAMP and GEONET on 29 November 2007. Figures 4a–4f have nearly the same format as Figure 1, but Figure 4d presents GEONET TEC fluctuations resampled along the CHAMP track. The color map in Figure 4g presents TEC detrended with 60 min moving window. The thick vertical lines in Figure 4g mark the CHAMP orbit.

The positive peaks in TEC deviations (Figure 4d) are generally collocated with negative peaks in in situ plasma density deviations (Figure 4c). In other words, there is a substantial phase difference between the TEC deviations and the in situ plasma density deviations. The background TEC is about 6–7 TECU (total electron content unit, 1 TECU = 10^{16} el m^{-2}) in GEONET data (figure not shown), and the peak-to-peak amplitude of TEC fluctuations is about 0.3 TECU as shown in Figure 4d. This yields relative TEC fluctuation levels of about 4–5%, which is similar to that of in situ plasma density fluctuations in Figure 4c (near 38–42°GLAT).

In summary, Figure 4 reveals that the GEONET TEC fluctuations, resulting mainly from around *F* peak heights, exhibit comparable amplitudes and wavelengths to those of CHAMP n_e observations. This feature in turn suggests that the n_e fluctuations are present over a range between around the *F* peak height and the CHAMP altitude. The phase difference between GEONET TEC and CHAMP-n_e in Figure 4 is as expected by *Onishi et al.* [2009]. Figure 1 of that paper also reveals nearly antiphase relationship between TEC and in situ n_e fluctuations. *Onishi et al.* [2009, Figure 3] suggest that the height-dependent phase difference should be determined by (1) the bottom altitude of collisionless ionospheric regime (assumed to be 450 km by *Onishi et al.* [2009]), (2) the altitude of maximum plasma density fluctuation (assumed to be 300 km by *Onishi et al.* [2009]), (3) tilt angle of the TGW wavefronts from vertical direction, and (4) altitude of the in situ plasma density observation (i.e., satellite altitude). As there are too many unknown parameters involved, the observed phase difference between the GEONET TEC and CHAMP-n_e cannot constrain them all simultaneously. Furthermore, opposite vertical gradients of plasma density above and below the *F* region peak height, which were not addressed in depth in *Onishi et al.* [2009, Figure 3] can further complicate the problem. Future work using satellite observations

and supporting computer simulations, which can impose further constraints on the relevant parameters, is warranted. As a first step toward this aim, Suzuki et al. (manuscript in preparation, 2015) investigate phase relation between MSTIDs observed at different altitudes.

4.3. Comparison With Previous Studies

Figures 2 and 3 generally agree with the climatology of in situ neutral mass density undulations shown in *Park et al.* [2014] for the following points: (1) the winter hemisphere exhibits higher activity (with relative fluctuation levels of approximately 0.1–1%) than the summer hemisphere during solstices, and (2) activity near the Andes during June solstice is stronger than at any other location and season. However, clear continent/ocean differences around the equator, which are quite prominent in *Park et al.* [2014] (especially during equinoxes and December solstice), cannot be identified easily in Figures 2 and 3. We speculate that steep n_e gradients related with daytime EIA structures, which are commonly observed at CHAMP altitudes generating artificial undulations when high-pass filtered, may hide weak tropical TGW signatures in n_e. Therefore, we refrain from drawing firm conclusions about activity at equatorial regions. This topic may be addressed in future works using satellite observations with lower orbit inclination angle, for which steep EIA walls should be less prominent.

Park et al. [2014] showed that thermospheric undulations at CHAMP altitudes have similar global distributions to those of stratospheric gravity waves, which supports the connection between the two. Similarly, the overall agreement between the global distributions of plasma density undulations in our study and *Park et al.* [2014, and references therein] in each season suggests that the former originates from gravity waves in the stratosphere, which are often attributed to orography and convective events [e.g., *Hoffmann et al.*, 2013; *Ern et al.*, 2011]. Those authors claimed the stronger jet stream as the reason for the enhanced stratospheric gravity wave activity during local winter.

On the other hand, terminator waves can also generate MSTIDs and affect a few local time hours around the terminators [*Afraimovich*, 2008; *Afraimovich et al.*, 2009]. Similarly, MSTIDs at auroral latitudes, which can be attributed to Joule heating and/or particle precipitation, may propagate to midlatitude/low-latitude regions [*Ishida et al.*, 2008, and references therein]. As typical MSTIDs have wavelengths of the order of 100 km [*Tsugawa et al.*, 2007, Table 1], the terminator and auroral activities may affect the wave amplitude distribution of our Figures 2 and 3. However, the conspicuous GLON dependence of our wave amplitude distribution cannot easily be attributed to the effects of terminator waves or auroral activities. In addition, we do not find any conspicuous indication in Figures 2 and 3 that auroral zone wave activity propagates below 60° MLAT in the summer hemisphere. Further, there have been debates as to how far auroral MSTIDs can propagate equatorward. *Ishida et al.* [2008] suggested that daytime MSTIDs at auroral latitudes can propagate to midlatitude regions. However, *Ishida et al.* [2008] also admitted that their observations could be interpreted alternatively as MSTIDs generated separately at midlatitudes and auroral regions.

Figures 2 and 3 generally agree with previous climatologies of daytime MSTIDs reported by *Kotake et al.* [2006] and *Otsuka et al.* [2013]. According to both papers, daytime MSTIDs occur preferentially in the winter hemisphere, which is consistent with our results. *Kotake et al.* [2006] further demonstrated that daytime MSTID activity does not strongly depend on solar activity, which agrees with the comparable fluctuation levels in our Figures 2 and 3. On the contrary, neutral density perturbation level in the upper thermosphere is known to be higher for lower solar activity, approximately by a factor of 2 [*Park et al.*, 2014]. We therefore speculate that the efficiency of neutral perturbations creating ionospheric undulations be lower for lower solar activity. According to *Kelley* [2009, equation (2.29a)], the ion-neutral collision frequency has a positive dependence on neutral and electron number density. Overall, plasma and neutral densities at CHAMP altitudes are higher for higher solar activity [e.g., *Lühr and Xiong*, 2010; *Lei et al.*, 2013]. Hence, the ion-neutral collision frequency and consequently the ion-neutral coupling efficiency are expected to be higher during active years. With a closer ion-neutral coupling, TGWs can be more efficient in driving ionospheric perturbations through plasma transport and redistribution. This effect seems to compensate for the smaller amplitudes of neutral density perturbations during solar maximum years. We regard this as the reason for the relative insensitivity of TGW-related n_e undulation levels to solar activity.

Nakanishi et al. [2014] presented a climatology of daytime magnetic field fluctuations, which they attributed to AGWs and related field-aligned currents (FACs). However, the general climatology of their wave distribution is quite different from our results. For example, *Nakanishi et al.* [2014, Figures 8 and 9] find highest activities generally at low latitudes (about 15° MLAT) while in our case amplitudes peak at midlatitudes (see our

Figures 2 and 3). We also find different seasonal dependences. These differences can be explained by the generation process. According to *Nakanishi et al.* [2014] AGWs propagating upward from the troposphere drive a dynamo effect in the *E* layer, which causes electric fields and FACs in the *F* region at CHAMP altitudes. Therefore, the signal strength depends strongly on the tropospheric source location and activity of AGWs and on the *E* region conductivity. Furthermore, the AGW climatology at *E* region altitudes, where the magnetic signatures are generated, may be different from the TGW climatology in the topside *F* layer (around CHAMP altitudes). Wave dissipation and secondary GW generation may be active between 90 and 140 km altitudes [e.g., *Vadas and Crowley*, 2010, Figure 14]. Therefore, although the primary AGW sources may be the same, the magnetic field perturbations of *Nakanishi et al.* [2014] and plasma density undulations in this study are expected to differ from each other.

Retterer and Roddy [2014] analyzed daytime plasma density fluctuations at near-equatorial regions using the Communication/Navigation Outage Forecast System (C/NOFS). Their Figure 7 shows that daytime equatorial $|\delta n_e/n_e^{\text{background}}|$ exhibits wave number 4 longitudinal structures during June solstice for low solar activity. On the contrary, the wave number 4 signatures are not identifiable for near-equatorial regions in our Figure 2. Several factors may contribute to the difference between our study and *Retterer and Roddy* [2014]. First, the difference can be attributed to methods of data analysis: *Retterer and Roddy* [2014] did not consider in situ neutral mass density fluctuations as one of the event selection criteria. Second, difference in orbital geometry of C/NOFS and CHAMP can also be considered as a contributor. CHAMP passes through the EIA in north-south directions, sampling the steep latitudinal gradient of plasma density (see the northern EIA edge around 25°N in Figure 1b). On the contrary, C/NOFS passes through the EIA approximately in east-west directions, scanning through different local times, which is more favorable for detecting tidal signatures. Third, there is a difference in scale sizes between *Retterer and Roddy* [2014, Figure 7] and our results, partly due to different data rates of the two satellites (CHAMP and C/NOFS). *Retterer and Roddy* [2014] defined $n_e^{\text{background}}$ as scale lengths of $\geq$ 300 km and analyzed the residual fluctuations, while we study scale lengths of 75–600 km. Fourth, it is also possible that TGWs observed along a north-south track (CHAMP) and those along an east-west track (C/NOFS) may have inherently different distributions. More studies are needed to clarify this issue.

4.4. Implications for EPB Climatology

Our results were obtained using daytime CHAMP observations up to sunset (18 LT). But the climatology of plasma density undulations shown in Figures 2 and 3 is quite different from that of postsunset EPBs [e.g., *Su et al.*, 2006]. For example, South America is nearly void of EPBs during June solstice [e.g., *Su et al.*, 2006, Figure 3] while it is the hottest spot of dayside n_e undulations related to ρ variation (see our Figures 2 and 3).

The climatology of low-latitude tropospheric convection activity presented by *Su et al.* [2014] and that of TGW in *Park et al.* [2014], both of which can be the source of n_e fluctuations in our Figures 2 and 3, are different from the general EPB climatology shown in previous studies. Based on these results, one may pose the question whether AGW and related plasma density undulation are among the dominant controlling factors of the EPB climatology, as occasionally assumed (see discussions in *Su et al.* [2014]).

Admittedly, CHAMP measures n_e fluctuations along its north-south orbit track while many studies have emphasized the role of n_e fluctuations along the east-west direction in EPB seeding (that is, large-scale wave structures with typical zonal wavelengths of 100–700 km) [e.g., *Thampi et al.*, 2009, and references therein]. According to *Retterer and Roddy* [2014, Figure 7], however, distributions of n_e fluctuations along the east-west direction also do not match the well-known EPB climatology. That is, the general climatology of daytime n_e fluctuations does not support the idea that seeding alone takes the dominant control of the EPB climatology. *Wu et al.* [2015] suggested that not only the existence of seeding but also their phasing is important for EPB seeding. This argument should be further explored in future model simulations.

5. Summary and Conclusion

In this study we analyzed daytime fluctuations in neutral mass density (ρ) and plasma density (n_e) measured onboard CHAMP from 2001 to 2010. We only consider n_e fluctuation events with high cross correlation with ρ. From our observations we could draw the following conclusions:

1. We confirm that there exist daytime fluctuations in n_e strongly correlated with in situ undulations of ρ. This can be considered as a strong support that the n_e fluctuations are generated in situ by neutral density variations.

2. The n_e fluctuations correlated with ρ exhibit the following climatological features: (1) they are generally stronger in the winter than in the summer hemisphere, and (2) amplitudes above South America in June solstice are larger than at any other location and season. The climatology of the n_e fluctuations is in general agreement with that of neutral mass density undulations shown by *Park et al.* [2014].
3. The relative amplitude of n_e fluctuations correlated with ρ does not depend strongly on solar activity. This result is in agreement with that of daytime MSTIDs as reported previously [*Kotake et al.*, 2006].

Acknowledgments
We sincerely thank Shin Suzuki and Hyosub Kil for helpful discussions on daytime plasma undulations. The CHAMP mission was sponsored by the Space Agency of the German Aerospace Center (DLR) through funds of the Federal Ministry of Economics and Technology. The site for CHAMP data distribution is http://isdc.gfz-potsdam.de/. J. Park was partially supported by the "Planetary system research for space exploration" project, the basic research funding from KASI, and the Air Force Research Laboratory, under agreement FA2386-14-1-4004.

Alan Rodger thanks the reviewers for their assistance in evaluating this paper.

References

Afraimovich, E. L. (2008), First GPS-TEC evidence of wave structure excited by solar terminator, *Earth Planets Space*, *60*, 895–900.
Afraimovich, E. L., I. K. Edemskiy, A. S. Leonovich, L. A. Leonovich, S. V. Voeykov, and Y. V. Yasyukevich (2009), MHD nature of night-time MSTIDs excited by the solar terminator, *Geophys. Res. Lett.*, *36*, L15106, doi:10.1029/2009GL039803.
Ern, M., P. Preusse, J. C. Gille, C. L. Hepplewhite, M. G. Mlynczak, J. M. Russell III, and M. Riese (2011), Implications for atmospheric dynamics derived from global observations of gravity wave momentum flux in stratosphere and mesosphere, *J. Geophys. Res.*, *116*, D19107, doi:10.1029/2011JD015821.
Fedorenko, A. K. (2010), Energy balance of acoustic gravity waves above the polar caps according to the data of satellite measurements, *Geomag. Aeron.*, *50*(1), 111–122.
Fedorenko, A. K., and E. I. Kryuchkov (2014), Observed features of acoustic gravity waves in the heterosphere, *Geomag. Aeron.*, *54*(1), 116–123.
Fedorenko, A. K., A. V. Bespalova, O. K. Cheremnykh, and E. I. Kryuchkov (2015), A dominant acoustic-gravity mode in the polar thermosphere, *Ann. Geophys.*, *33*, 101–108, doi:10.5194/angeo-33-101-2015.
Forbes, J. M., S. L. Bruinsma, Y. Miyoshi, and H. Fujiwara (2008), A solar terminator wave in thermosphere neutral densities measured by the CHAMP satellite, *Geophys. Res. Lett.*, *35*, L14802, doi:10.1029/2008GL034075.
Goodwin, L. V., et al. (2015), Swarm in situ observations of F region polar cap patches created by cusp precipitation, *Geophys. Res. Lett.*, *42*, 996–1003, doi:10.1002/2014GL062610.
Hocke, K., K. Schlegel, and G. Kirchengast (1996), Phases and amplitudes of TIDs in the high-latitude F-region observed by EISCAT, *J. Atmos. Terr. Phys.*, *58*, 245–255.
Hoegy, W. R., L. H. Brace, W. T. Kasprzak, and C. T. Russell (1990), Small-scale plasma, magnetic, and neutral density fluctuations in the nightside Venus ionosphere, *J. Geophys. Res.*, *95*(A4), 4085–4102, doi:10.1029/JA095iA04p04085.
Hoffmann, L., X. Xue, and M. J. Alexander (2013), A global view of stratospheric gravity wave hotspots located with Atmospheric Infrared Sounder observations, *J. Geophys. Res. Atmos.*, *118*, 416–434, doi:10.1029/2012JD018658.
Ishida, T., K. Hosokawa, T. Shibata, S. Suzuki, N. Nishitani, and T. Ogawa (2008), SuperDARN observations of daytime MSTIDs in the auroral and mid-latitudes: Possibility of long-distance propagation, *Geophys. Res. Lett.*, *35*, L13102, doi:10.1029/2008GL034623.
Johnson, F. S., W. B. Hanson, R. R. Hodges, W. R. Coley, G. R. Carignan, and N. W. Spencer (1995), Gravity waves near 300 km over the polar caps, *J. Geophys. Res.*, *100*(A12), 23,993–24,002, doi:10.1029/95JA02858.
Kelley, M. C. (2009), *The Earth's Ionosphere: Plasma Physics and Electrodynamics*, Academic Press, San Diego, Calif.
Kil, H. (2015), The morphology of equatorial plasma bubbles: A review, *J. Astron. Space Sci.*, *32*(1), 13–19.
Kotake, N., Y. Otsuka, T. Tsugawa, T. Ogawa, and A. Saito (2006), Climatological study of GPS total electron content variations caused by medium-scale traveling ionospheric disturbances, *J. Geophys. Res.*, *111*, A04306, doi:10.1029/2005JA011418.
Kotake, N., Y. Otsuka, T. Ogawa, T. Tsugawa, and A. Saito (2007), Statistical study of medium-scale traveling ionospheric disturbances observed with the GPS networks in Southern California, *Earth Planets Space*, *59*, 95–102.
Lei, J., G. Chen, X. Jiyao, and X. Dou (2013), Impact of solar forcing on thermospheric densities and spacecraft orbits from CHAMP and GRACE, Geodetic Sciences—Observations, Modeling and Applications, doi:10.5772/56599. [Availabe at http://cdn.intechopen.com/pdfs-wm/44516.pdf.]
Liu, H., H. Lühr, and S. Watanabe (2009), A solar terminator wave in thermospheric wind and density simultaneously observed by CHAMP, *Geophys. Res. Lett.*, *36*, L10109, doi:10.1029/2009GL038165.
Lübken, F.-J., G. Lehmacher, T. Blix, U.-P. Hoppe, E. Thrane, J. Cho, and W. Swartz (1993), First in-situ observations of neutral and plasma density fluctuations within a PMSE layer, *Geophys. Res. Lett.*, *20*, 2311–2314.
Lühr, H., and C. Xiong (2010), IRI-2007 model overestimates electron density during the 23/24 solar minimum, *Geophys. Res. Lett.*, *37*, L23101, doi:10.1029/2010GL045430.
Lühr, H., M. Rother, W. Köhler, P. Ritter, and L. Grunwaldt (2004), Thermospheric up-welling in the cusp region: Evidence from CHAMP observations, *Geophys. Res. Lett.*, *31*, L06805, doi:10.1029/2003GL019314.
Morgan, M. G. (1990), Daytime traveling ionospheric disturbances observed at $L \approx 4.5$ in western Quebec with rapid-run ionosondes, *Radio Sci.*, *25*(1), 73–83, doi:10.1029/RS025i001p00073.
Nakanishi, K., T. Iyemori, K. Taira, and H. Lühr (2014), Global and frequent appearance of small spatial scale field aligned currents possibly driven by the lower atmospheric phenomena as observed by the CHAMP satellite in middle and low latitudes, *Earth Planets Space*, *66*, 40, doi:10.1186/1880-5981-66-4.
Nicolls, M. J., and C. J. Heinselman (2007), Three-dimensional measurements of traveling ionospheric disturbances with the Poker Flat Incoherent Scatter Radar, *Geophys. Res. Lett.*, *34*, L21104, doi:10.1029/2007GL031506.
Nishioka, M., T. Tsugawa, M. Kubota, and M. Ishii (2013), Concentric waves and short-period oscillations observed in the ionosphere after the 2013 Moore EF5 tornado, *Geophys. Res. Lett.*, *40*, 5581–5586, doi:10.1002/2013GL057963.
Nygrén, T., A. T. Aikio, M. Voiculescu, and L. Cai (2015), Radar observations of simultaneous traveling ionospheric disturbances and atmospheric gravity waves, *J. Geophys. Res. Space Physics*, *120*, 3949–3960, doi:10.1002/2014JA020794.
Onishi, T., T. Tsugawa, Y. Otsuka, J.-J. Berthelier, and J.-P. Lebreton (2009), First simultaneous observations of daytime MSTIDs over North America using GPS-TEC and DEMETER satellite data, *Geophys. Res. Lett.*, *36*, L11808, doi:10.1029/2009GL038156.
Otsuka, Y., K. Suzuki, S. Nakagawa, M. Nishioka, K. Shiokawa, and T. Tsugawa (2013), GPS observations of medium-scale traveling ionospheric disturbances over Europe, *Ann. Geophys.*, *31*, 163–172, doi:10.5194/angeo-31-163-2013.
Park, J., H. Lühr, C. Lee, Y. H. Kim, G. Jee, and J.-H. Kim (2014), A climatology of medium-scale gravity wave activity in the midlatitude/low-latitude daytime upper thermosphere as observed by CHAMP, *J. Geophys. Res. Space Physics*, *119*, 2187–2196, doi:10.1002/jgra.50886.

Retterer, J. M., and P. Roddy (2014), Faith in a seed: On the origins of equatorial plasma bubbles, *Ann. Geophys.*, *32*, 485–498, doi:10.5194/angeo-32-485-2014.

Su, S.-Y., C. H. Liu, H. H. Ho, and C. K. Chao (2006), Distribution characteristics of topside ionospheric density irregularities: Equatorial versus midlatitude regions, *J. Geophys. Res.*, *111*, A06305, doi:10.1029/2005JA011330.

Su, S.-Y., W. Chung Lung, and C. H. Liu (2014), Correlation between the global occurrences of ionospheric irregularities and deep atmospheric convective clouds in the Intertropical Convergence Zone (ITCZ), *Earth Planets Space*, *66*, 134.

Thampi, S. V., M. Yamamoto, R. T. Tsunoda, Y. Otsuka, T. Tsugawa, J. Uemoto, and M. Ishii (2009), First observations of large-scale wave structure and equatorial spread F using CERTO radio beacon on the C/NOFS satellite, *Geophys. Res. Lett.*, *36*, L18111, doi:10.1029/2009GL039887.

Tsugawa, T., N. Kotake, Y. Otsuka, and A. Saito (2007), Medium-scale traveling ionospheric disturbances observed by GPS receiver network in Japan: A short review, *GPS Solut.*, *11*, 139–144, doi:10.1007/s10291-006-0045-5.

Vadas, S. L. (2007), Horizontal and vertical propagation and dissipation of gravity waves in the thermosphere from lower atmospheric and thermospheric sources, *J. Geophys. Res.*, *112*, A06305, doi:10.1029/2006JA011845.

Vadas, S. L., and G. Crowley (2010), Sources of the traveling ionospheric disturbances observed by the ionospheric TIDDBIT sounder near Wallops Island on 30 October 2007, *J. Geophys. Res.*, *115*, A07324, doi:10.1029/2009JA015053.

Vadas, S. L., and H.-L. Liu (2013), Numerical modeling of the large-scale neutral and plasma responses to the body forces created by the dissipation of gravity waves from 6 h of deep convection in Brazil, *J. Geophys. Res. Space Physics*, *118*, 2593–2617, doi:10.1002/jgra.50249.

Wu, T.-W., J. D. Huba, J. Krall, D. C. Fritts, and B. Laughman (2015), Seeding equatorial spread F with turbulent gravity waves: Phasing effects, *Geophys. Res. Lett.*, *42*, 15–21, doi:10.1002/2014GL062348.

Yokoyama, T., and D. L. Hysell (2010), A new Midlatitude Ionosphere Electrodynamics Coupling model (MIECO): Latitudinal dependence and propagation of medium-scale traveling ionospheric disturbances, *Geophys. Res. Lett.*, *37*, L08105, doi:10.1029/2010GL042598.

Yokoyama, T., H. Shinagawa, and H. Jin (2014), Nonlinear growth, bifurcation and pinching of equatorial plasma bubble simulated by three-dimensional high-resolution bubble model, *J. Geophys. Res. Space Physics*, *119*, 10,474–10,482, doi:10.1002/2014JA020708.